Detection and labeling ribs on expiration chest radiographs

Mira Park[a], Jesse S. Jin[a,b], and Laurence S. Wilson[c]

[a]Computer Science and Engneering, University of New South Wales, NSW 2052, Australia
[b]School of Information Technologies, University of Sydney, NSW 2006, Australia
[c]Telecommunicatons and Industrial Physics, CSIRO, NSW 1710, Australia

ABSTRACT

Typically, inspiration is preferred when xraying the lungs. The x-ray technologist will ask a patient to be still and to take a deep breath and to hold it. This not only reduces the possibility of a blurred image but also enhances the quality of the image since air-filled lungs are easier to see on x-ray film. However, inspiration causes low density in the inner part of lung field. That means that ribs in the inner part of lung field have lower density than the other parts nearer to the border of the lung field. That is why edge detection algorithms often fail to detect ribs. Therefore to make rib edges clear we try to produce an expiration lung field using a 'hemi-elliptical cavity'. Based on the expiration lung field, we extract the rib edges using *canny edge detector* and a new connectivity method, called '4 way with 10-neighbors connectivity' to detect clavicle and rib edge candidates. Once the edge candidates are formed, our system selects the best candidates using knowledge-based constraints such as a gradient, length and location. The edges can be paired and labeled as superior rib edge and inferior rib edge. Then the system uses the clavicle, which is obtained in a same method for the rib edge detection, as a landmark to label all detected ribs.

Keywords: chest radiograph, medical image, detection ribs, labeling ribs, expiration, hemi-elliptical cavity, 4 way with 10 neighbors connectivity

1. INTRODUCTION

The ribs in chest radiographs are essential structures of the osseous thorax and provide information that aids in the interpretation of a radiologic image [1]. Techniques for making precise identification of the ribs are useful in detection of rib lesions and localization of lung lesions. The clavicle may be used as anatomic landmark for chest radiographs.

Since 1970s, many methods to detect ribs automatically were proposed. Toriwaki *et al.* [2] in 1973 attempted to use template matching and assumed that all ribs had the same width and were equally spaced. Wechsler *et al.* [3] used a high-pass filter to enhance the edges, a combination of thresholding, Laplacian and gradient operators to detect the local edges, a Hough technique to detect straight lines and several concepts of artificial intelligence (i.e., heuristic reasoning schemes) through an elaborate rib model consisting of a combination of parabolas and elliptical curves to select rib edges from the detected edges. Powell *et al.* [4] fitted a shift-variant function to two vertical profiles in the periphery of both lungs to obtain estimates of locations of rib edges. The method was refined by analyzing cumulative edge gradients and their orientation in small regions-of-interests (ROIs) that are located adjacent to the initially estimated edges [5]. Sun [6] used *a pirori* knowledge, which is provided through a model of the object, to identify and locate the ribs through comparing the input image and the model. Yue *et al.* [7] fitted parabolas to edge pixels with a Hough transform, used simple rules to discriminate 'true' maxima in the Hough space from 'false' responses and refined the location of the rib borders with snakes. Sugahara *et al.* [8] calculated the intensity of the edges of an input image using a derivative filter and the possibility of lines and arcs using Hough transformation to make a structural edge map consisting of subclaviculars, heart, diaphrgam, and ribs. Vogelsang *et al.* [9] detected the rib borders by applying a filtering operation in the frequency domain to emphasize the high frequency parts of the image signal, a Hough transform on the image and a network approach to detect the rib structures and borders. Ginneken *et al.* [10] developed a statistical shape model for the complete rib cage and fitted the global rib cage directly to the radiograph. Li *et al.* [11] developed a model based detection technique for rib edges using a generalized Hough transform technique and a snake model technique.

Medical Imaging 2003: Physics of Medical Imaging, M. J. Yaffe, L. E. Antonuk,
Editors, Proceedings of SPIE Vol. 5030 (2003) © 2003 SPIE · 1605-7422/03/$15.00

The above proposed approaches have general steps as follows:

1. Preprocessing using a low pass filter (Gaussian filter), a high pass filter or a gradient operator (i.e., Sobel operator or Roberts operator),
2. Producing rib border candidates using Hough transform or model (i.e., parabolas, elliptical curves or statistical shape),
3. Determining the best candidates using a simple rule or heuristic reasoning schemes,
4. Refining the edge using an active contour model or edge gradients.

In preprocessing, Daponte *et al.* [12] indicated the Sobel operator appears to be more suitable for processing chest radiographs than the Roberts operator and the most efficient procedure was to filter the image with the Gaussian filter approximation before applying the Sobel operation. The gradient operators are a conceptually tractable and computationally effective means to enhance edges of objects. However, since the edges are emphasized, we usually obtain two lines for one edge when we apply any *edge detector* to detect the edges on an image. This effect is certainly not desired as we require one line for one edge. Therefore, the common radiographic procedures, which are low pass filter (i.e., Gaussian filter) to reduce noise and the gradient operators or a high-pass filter to emphasize the rib edges in chest radiograph, is not suitable for our algorithm.

There is another obstacle when detecting the rib edges. The ribs at the inner part of the lung field are not clearer than the boundary area of the lung field because the inner part of the lung field is usually darker than those parts which are nearer to the boundary. This happens because of the typical chest radiograph procedure. The x-ray technologist will typically ask the patient to be still, to take a deep breath and to hold it. This not only reduces the possibility of a blurred image but also enhances the quality of the image since air-filled lungs are easier to see on x-ray film than deflated lungs. When x-rays penetrate the body, they are absorbed in varying amounts by different parts of the anatomy. Ribs will absorb much of the radiation and therefore, appear white or light gray on the image. However, the air-filled lungs reduce the intensity of the ribs, especially in the inner part of the lung field. This means that ribs in the inner part of lung field have a lower density than the other parts nearer to the boundary of the lung field. That is why the edge detection algorithm often fails to detect ribs in those areas.

Therefore, we need to emphasis the ribs in the inner part of the lung more than the ribs at the boundary area. We emphasis the ribs at the middle of the lung field with maximum weight and the weight is gradually reduced towards the boundary of the lung field.

In this paper, to make rib edges clear we simply try to produce an expiration lung field. We use the 'ellipsoid' concept to achieve this, so we call the operation 'hemi-ellipsoid cavity'. Based on the expiration lung field, we extract the rib edges use *canny edge detector* and a new connectivity method, called '4 way with 10 neighbors connectivity', to form clavicle and rib edges. We then label the ribs using the clavicles as landmarks.

The layout of this paper is as follows. In Section 2, we introduce a new rib border emphasis method and in Section 3, we propose the rib border detection algorithm. In Section 4, we present the rib labeling and we analyze the performance in Section 5. The conclusion is presented in Section 6.

2. EMPHASIS OF RIB BORDERS

2.1. Hemi-elliptical cavity

The center of the ellipsoid is (x_0, y_0). We form the equation (Figure 1(a)) as follows,

$$\frac{(x-x_0)^2 -}{a^2} + \frac{(y-y_0)^2}{b^2} + \frac{z^2}{c^2} = 1 \qquad (1)$$

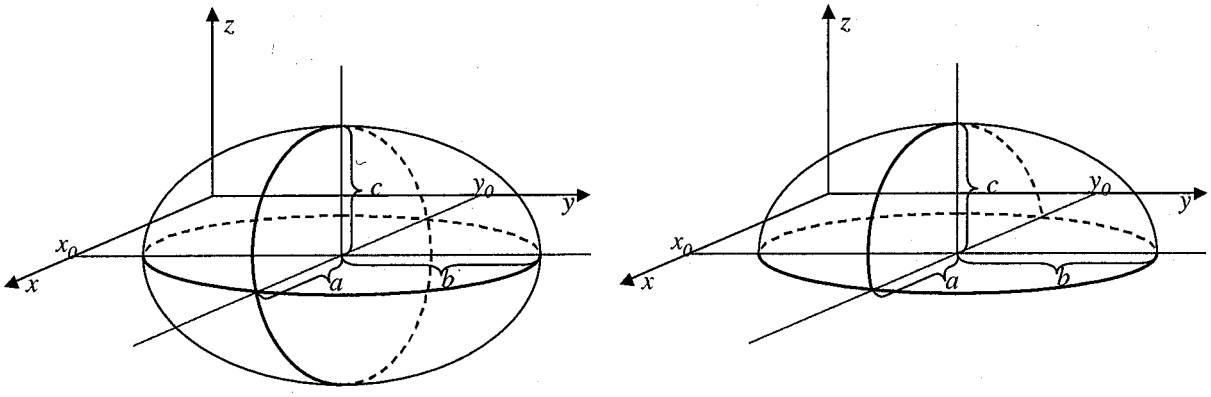

(a) (b)

Figure 1. The model of an ellipsoid

The z surface values are needed to form a hemi-elliptical cavity, so the following equation is derived from equation (1).

$$z^2 = c^2 \times \left(1 - \frac{(x - x_0)^2}{a^2} - \frac{(y - y_0)^2}{b^2}\right) \tag{2}$$

We assume $z >= 0$ (Figure 1(b)). a, b and c are constant values, which should be decided by the lung shape. First, the center point (x_0, y_0) of the ellipsoid is the center of the lung (Figure 2) and radii of the ellipsoid are obtained from the lung width, height and center intensity value. That means the first component $\boldsymbol{a}$ is the half length of the lung width, the second component $\boldsymbol{b}$ is the half length of the lung height and the third component $\boldsymbol{c}$ is the intensity value at $f(x_0,y_0)$ where f is the input chest radiograph. We reform the equation for convenience as follows.

$$v(x_i, y_i) = \sqrt{f(x_0, y_0)^2 \times \left(1 - \frac{(x_i - x_0)^2}{a^2} - \frac{(y_j - y_0)^2}{b^2}\right)} \tag{3}$$

where i is 1 to n and j is 1 to m when the size of the input chest radiograph is $n \times m$. We form a hemi-elliptical cavity with the values, $v(x_i, y_i)$, when they are greater than 0 or equal to 0. Figure 2 shows the example of a hemi-elliptical cavity on a chest radiograph.

2.2 Expiration chest radiograph

We add a hemi-elliptical cavity to deflate a lung using the following condition.

$$\begin{aligned} &\textit{if} \quad v(x_i, y_i) >= 0 \\ &\qquad f'(x_i, y_j) = f(x_i, y_j) + v(x_i, y_i) \\ &\textit{else} \\ &\qquad f'(x_i, y_j) = f(x_i, y_j) \end{aligned} \tag{4}$$

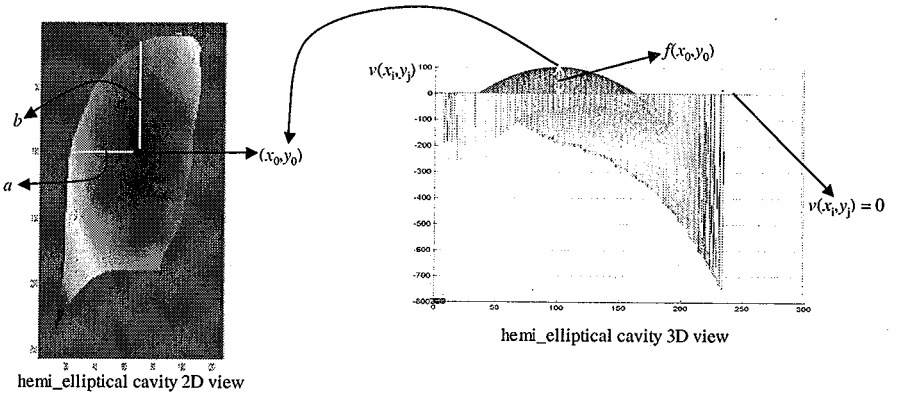

Figure 2. hemi-elliptical cavity

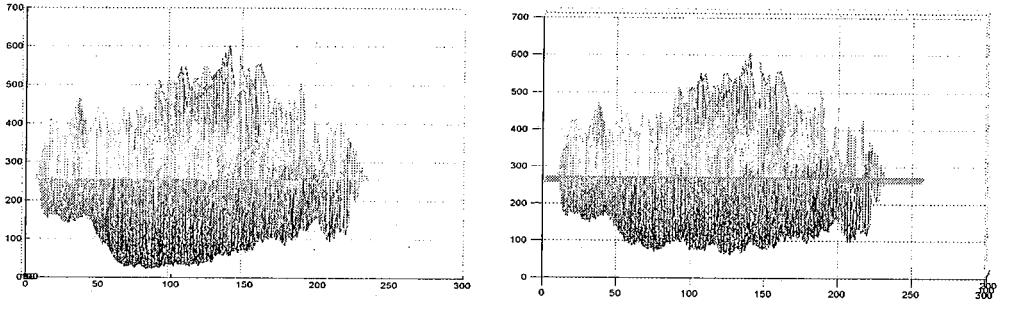

(a) The input (inspiration) lung image

(b) The expiration lung image

Figure 3. The 3D view of the lung field before and after deflation

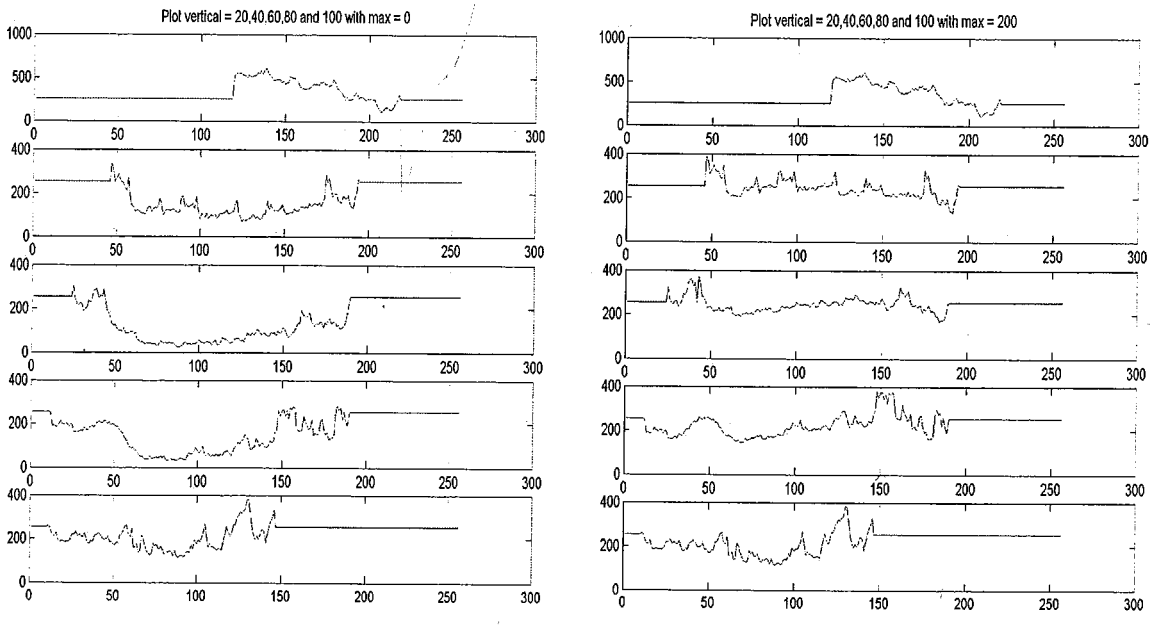

(a) The input (inspiration) lung field

(b) The expiration lung field

Figure 4. Plot the column data at $x = 20$, 40, 60, 80 and 100 before and after deflation of the lung

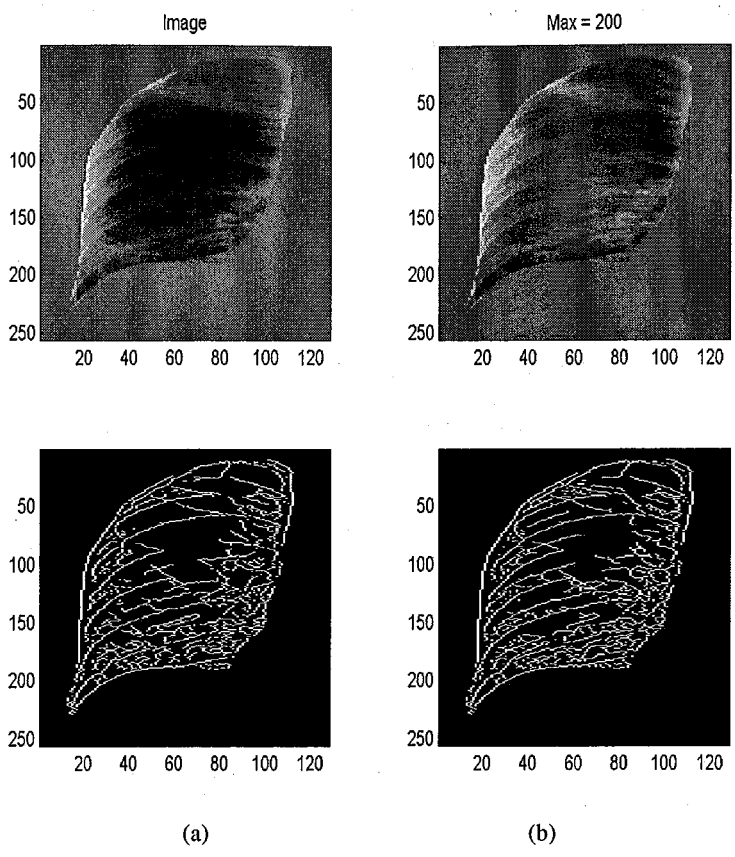

Figure 5. (a) The input lung field and its edges (b) The expiration lung field and its edges

Figure 3. shows the 3 dimensions view of the lung filed before and after deflation by plotting the intensity values. The left of the graphs is the apex of the lung and the right side is the hemi-diaphragm of the lung. The middle of the lung field in Figure 3(a) has a round shape and Figure 4(a) shows the roundness more clearly. It plots the intensity value along the column 20, 40, 60, 80 and 100. The middle intensity values at column 40, 60 and 80 are lower than other areas. Therefore, we deflated that area using a hemi-elliptical cavity to reduce the intensity of the middle of the lung with weighting. Figure 3(b) and Figure 4(b) also present the revised shape without the texture changes. Figure 5 demonstrates the 2-D chest radiograph and its edges detected using *canny edge detection* algorithm.

3. DETECTION OF RIB BORDERS

Our approach to object recognition differs from many others in that the segmentation and matching processes are combined to a large extent [13,14]. Segmentation is carried out to locate a specified anatomical structure and is restricted using domain knowledge. Thus the system already knows what label an image primitive may be assigned even before it has segmented it. This model-driven approach is possible for medical images because their contents are well-defined. While there are variations in image acquisition parameters, such as the intensity of an X-ray beam or the position of a patient, they are not as significant as variations in camera positioning or lighting which may effect other computer vision systems. In problems where the image content is not known *a priori* to such an extent, the interpretation is usually more data-driven: unguided segmentation is performed, and only then is domain knowledge invoked to label the primitives.

3.1 Set of the edge candidates from the image point primitive

We have applied Canny [16] edge detectors to extract line primitives from 2-D chest radiographs. Typically the expected anatomical structures do not produce a single, continuous edge. The system generates candidates by

connecting the continuous sets of points. Connectivity between pixels is an important concept used in establishing boundaries of objects and components of regions in an image. To establish whether two pixels are connected, it must be determined if they are adjacent in some sense and if their gray levels satisfy a specified criterion of similarity. There are three types of connectivity [17]:

- 4-*connectivity*. Two pixels p and q with values from V are 4-connected if q is in the set $N_4(p)$.
- 8-*connectivity*. Two pixels p and q with values from V are 8-connected if q is in the set $N_8(p)$.
- m-*connectivity* (mixed connectivity). Two pixels p and q with values from V are m-connected if

  (i) q is in $N_4(p)$, or

  (ii) q is in $N_D(p)$ and the set $N_4(p) \cap N_4(q)$ is empty.

where V is the set of gray-level values used to define connectivity. However, using these connectivity methods on our image, we have two problems. First, since the rib edges and the clavicle edges have a certain gradient, length and location, these properties should be considered to produce rib edge candidates. In this sense, for the left lung rib edges, only 4 way can be linked with the current pixel such as direct left, right, left down, and right up neighbors. Secondly, it is important to consider the rib edges, which are often intervened by other structures such as vessels, so the neighbor's neighbor should be checked for links but the gradient also should be maintained.

In a binary image, $V = \{1\}$ for the connectivity of pixels with value 1, the paths between 8-neighbors of the pixel indicated by bold font are shown by dashed lines in Figure 6(b). The ambiguity in path connections that results from allowing 8-connectivity is removed by using m-connectivity, as shown in Figure 6(c). Figure 6(d), (e) show 4 way 10-neighbors connectivity for the left and the right lung. The indicated pixel has paths with neighbors within certain directions and neighbors' neighbor. A path from pixel p with coordinates (x, y) to pixel q with coordinates (s,t) is a sequence of distinct pixels with coordinates

$$(x_0, y_0), (x_1, y_1), \ldots, (x_n, y_n)$$

where $(x_0, y_0) = (x, y)$ and $(x_n, y_n) = (s,t)$, (x_i, y_i) is adjacent to (x_{i-1}, y_{i-1}), $1 \le i \le n$, and n is the *length* of the path. The 4 directions and 10 possible neighbors of our connectivity are shown in Figure 7. The allowable path degree is less than 45°, so it could be checked by:

$$\arctan\left(\left|\frac{y_n - y_0}{x_n - x_0}\right|\right) \le \frac{\pi}{4} \tag{5}$$

An outline of the selection of the candidates algorithms is as follows:

1. Calculate edge points, with their associated gradient magnitude and phase (direction) using *canny edge detector*
2. Apply magnitude and phase constraints, retaining only those points which satisfy the constrains
3. Form edge fragments from continuous sets of points using 4 way 10-neighbors connectivity
4. Calculate all possible linkages of edge fragments to form candidates: a linkage can occur if the end points of the fragments are close enough, and the angle between them is within the orientation constraint range
5. Discard all candidates which do not satisfy the length constraints: we select a minimum *length* to accept as an edge and we empirically selected a minimum length of 25 pixels

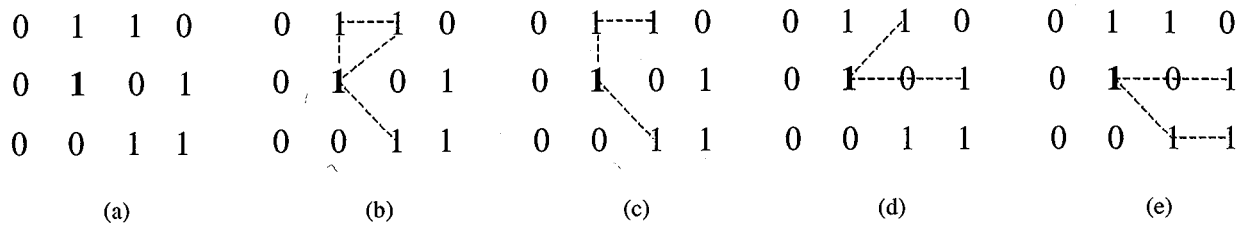

Figure 6. (a) Arrangement of pixels; (b) 8-neighbors of the bolded pixel; (c) m-neighbors of the same pixel; (d) 4 way with 10-neighbors of the bolded pixel for the left lung clavicle and the right lung ribs; (e) 4 way with 10-neighbors of the bolded pixel for the right lung clavicle and the left lung ribs

(a) For the right lung clavicle and the left lung ribs (b) For the left lung clavicle and the right lung ribs

Figure 7. 4 way with 10-neighbors connectivity

3.2 Selection of the best candidates

Once the edge candidates are formed, our system selects the best candidates using knowledge-based constraints such as gradient, length and location. The process to select the best candidates is as follows (see Figure 8)

1. Select the longest candidate (C_1) within a gradient, length constraint at the middle lung
2. Start to draw the semi-circle with a certain radius (r_1) from the beginning of C_1 to below C_1
3. Process the semi-circle along the edge (C_1) until it reaches the end of the edge
4. Check the length of the candidates within the area where the semi-circles are below C_1
5. Select the longest length candidate (C_2) within a gradient, length constraint and repeat the semi-circle operation with C_2
    - if there are no candidates within the constraint area, increase the semi-circle radius (r_1) and process the semi-circle operation again with C_1 until the process finds some candidates.
6. Repeat from 1 to 5 with a new candidate
7. When the process reaches the end of the lung, it goes back to C_1
8. Repeat the semi-circle operation above the C_1
9. Select the longest length candidate (C_5) and repeat the semi-circle operation until the process reaches the top of the lung

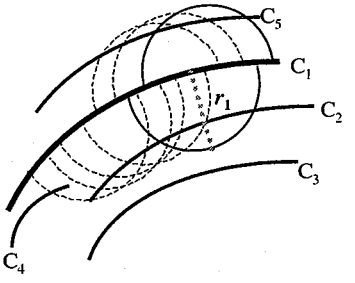

Figure 8. The semi-circle operation

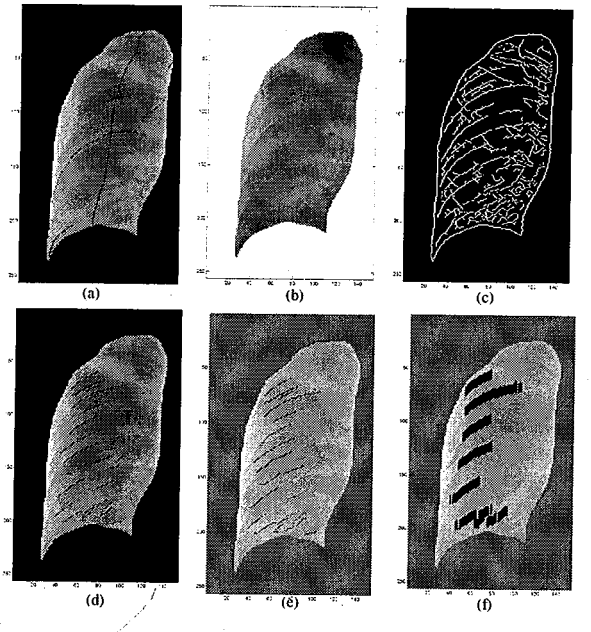

Figure 9. (a) Input image with the middle lines of the lung; (b) Expiration lung; (c) The edges of the expiration lung (d) The rib candidates (e) The best rib candidates (f) The mark from the inferior rib line

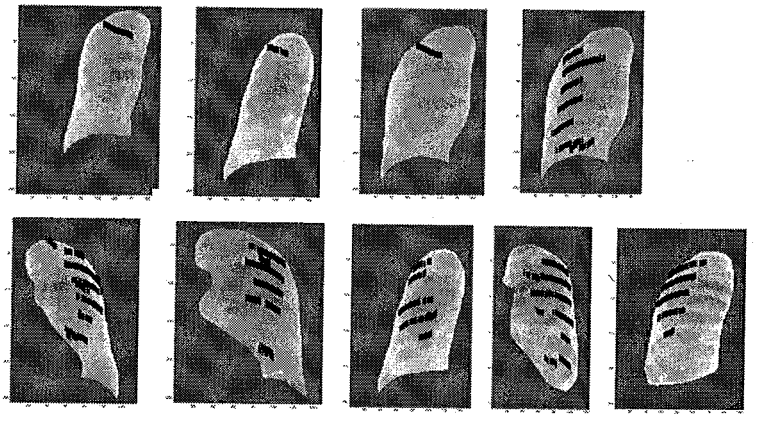

Figure 10. Detection of the inferior ribs and clavicles

The result is shown in Figure 9(e). Figure 9(f) shows the mark for the inferior rib edge. The superior rib edge is the top edge of the rib and the inferior edge is the bottom edge of the rib. We use the semi-circle operation to check the average intensity value above (*I(above)*) and below (*I(below)*) the edge. If *I(above)* is greater than *I(below)*, the system accepts the edge as an inferior rib edge since the ribs have higher intensity than other parts in the lung, so if the area above of the edge is more dense than the area below the edge, this means that above the edge is a rib and that below the edge is lung tissue. To make the result visible, our system marks with '0' the area 12 pixels up from the inferior rib edge (see Figure 9(f) and Figure 10).

4. LABELING OF THE RIBS

Once all the possible edges (candidates) are obtained from image processing, the edges can be paired and labeled as superior rib edge and inferior rib edge by applying knowledge-based constraints. The constraints use both *a priori* (model), and *a posteriori* (recognized anatomy) information. There are 4 knowledge constraint parameters, which are *strength* (gradient magnitude), *orientation* (gradient direction), *position* (image search area) and length. The *strength* of an edge primitive is determined from the image gradient magnitude at the edge points.

The system then uses the clavicle, which is obtained using the same method for the rib edge detection (see Figure 11), as a landmark to label all ribs. The clavicle usually crosses the 3rd rib first and crosses the 4th rib second. Therefore the system can label the first rib crossed by the beginning of the clavicle as a 3rd rib and the second rib crossed by the end of clavicle as a 4th rib. All distances should be checked from the 3rd rib or 4th rib to label the remaining ribs. (see Figure 11).

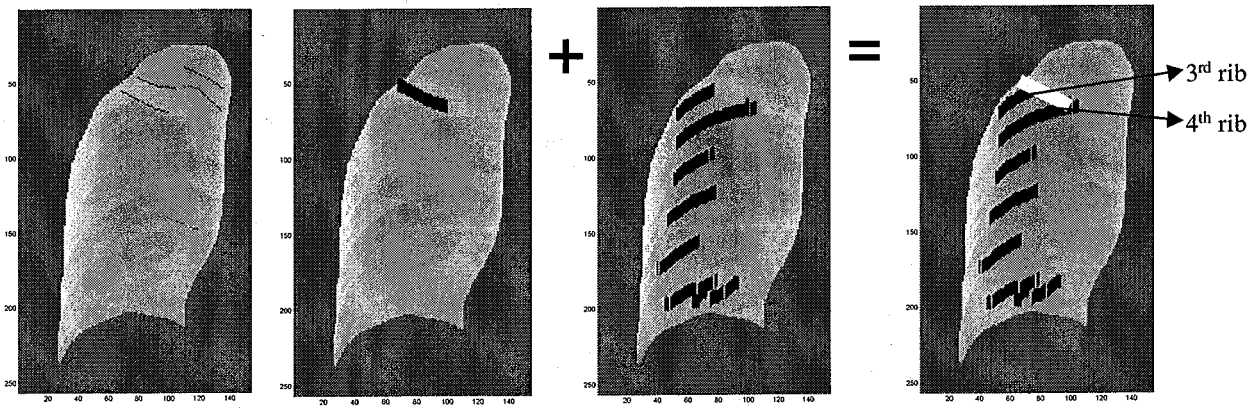

Figure 11. Labeling the 3rd and 4th ribs

5. PERFORMANCE ALALYSIS

We tested 35 standard Posteroanterior (PA) 14″×17″ chest radiographs, selected in the Department of Radiology, St Vincents Hospital. The radiographs were digitized with a Kodak Lumiscan Film Digitiser. The resolution of the digitized images is 0.175mm with matrix size of 2048 by 2486, and the images are subsampled to 256 by 300 to reduce the unnecessary points and edges that could be extracted. Our method applies to the segmented lung field using a lung field segmentation based on knowledge developed by Brown [13] and extended by Park [14]. A chest radiograph includes two lung fields, which are the right- and the left-lung, and we divide them into two sets. Therefore, there are 70 possible test cases which include 20 normal lung fields and 50 abnormal lung fields. 49 clavicles were identified from both normal and abnormal lung field and 42 cases succeeded to label the 3rd and 4th ribs from the 49 test cases, which included identification of the clavicle by the system.

6. CONCLUSION

In this paper, we proposed a new method to detect and label the ribs and the clavicles in the lung field. The rate for clavicle detection is 70% and the rate for rib labeling is 60%. The rate is quite reasonable even though the test does not consider any different circumstance for different cases. That means, the test should consider whether a radiologist is able to detect the clavicles and ribs in the chest radiographs, so it is sure the objects are clearly seen on the input images and they are expected to be detected by the system. Therefore, the evaluation could be with a five-point rating scale, that is from 1 (very poor), which is for the most ribs are not registered and appear in the entire intercostals space, to 5 (excellent), which is for all ribs are perfectly registered [15]. However, our test image database consists of normal chest radiographs as well as abnormal chest radiographs may include unclear presentation of the ribs and clavicles. Therefore, our system demonstrated a high possibility to detect and label the ribs and clavicles in a new way proposed in this paper.

Our system did not attempt to shape the whole rib structure, but the ribs and clavicles information provided by our system is very useful for the report about the rib abnormality. For example, our application for interpreting a chest radiograph (see Figure 12) uses this information to detect the rib intensity. It is worthwhile to check the intensity of the ribs since dense or sclerotic ribs may be sign of cancer or may indicate sickle cell disease, endstage renal disease, or other metabolic disease [7]. The numeric intensity value produced by our system is converted to s semantic word such as 'normal', 'abnormally high', and 'abnormally low' using fuzzy function. In Figure 12, rib intensity has been annotated as abnormally high indicating possible disease.

Furthermore, the labeled ribs and clavicles could be landmarks for other rib detection methods or image registration for chest radiograph.

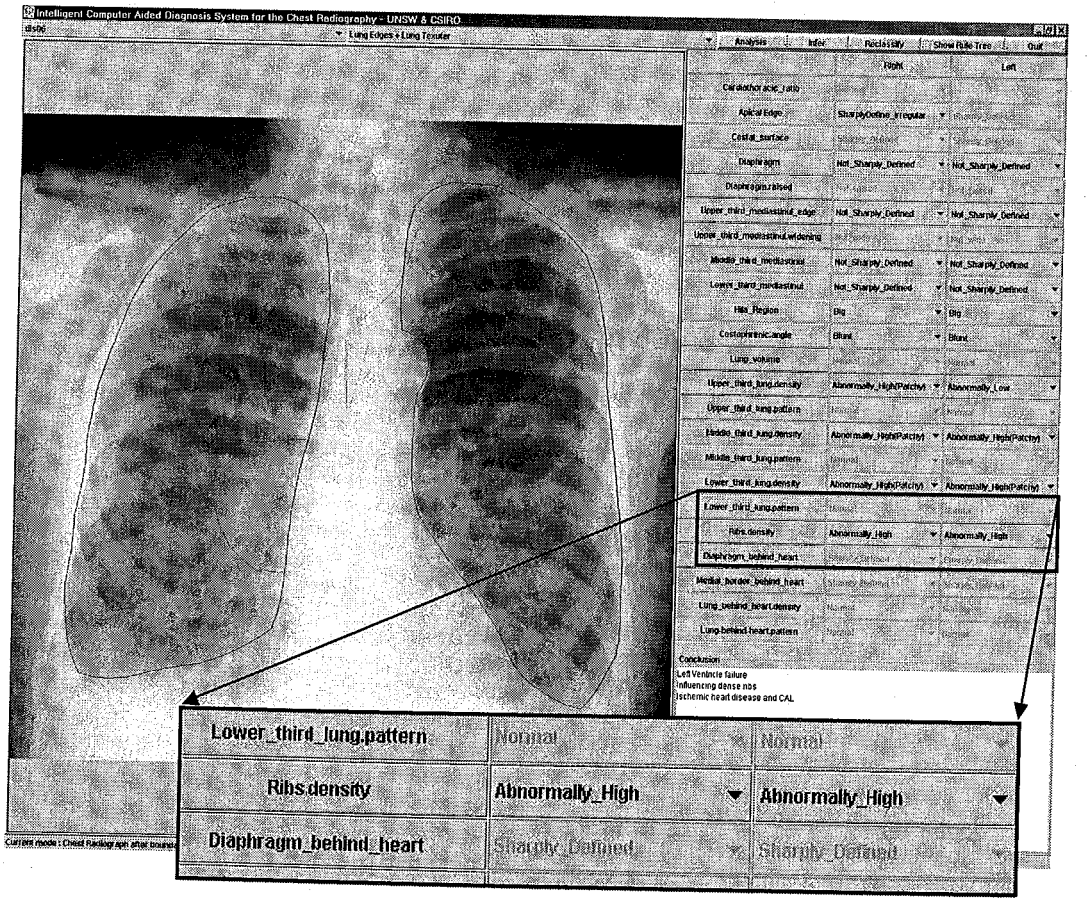

Figure 12. Computer Aided Diagnosis System for chest Radiographs

7. REFERENCES

1. Kurihara Y., Yahushiji K.Y., Matsumoto J., Ishikawa T. and Hirata K., "The Ribs: Anatomic and Radiologic Considerations", RadioGraphics, **19(1)**:105-119, 1999
2. Toriwaki J., Suenaga Y., Negoro T. and Fukumura T., "Pattern Recognition of Chest X-ray Images", Computer Graphics and Image Processing, **2**:252-271, 1973
3. Wechsler H. and Skansky, "Automatic Detectin of Rib Contours in Chest Radiographs", International Joint Conference on Artificial Intelligence, 688-694, 1975
4. Powell G.F., Doi K. and Katsuragawa S., "Localization of Inter-Rib Spaces for Lung Texture Analysis and Computer-Aided Diagnosis in Digital Chest Images. Medical Physics, **15(4)**:581-587, 1988
5. Sanada S., Doi K. and MacMahon H., "Image Feature Analysis and Computer-Aided Diagnosis in Digital Radiograph: Automated Delineation of Posterio Ribs in Chest Images", Medical Physics, **18(5)**:964-971, 1991
6. Sun C., "Image Processing in the Medical Image Understanding Project", CSIRO Institute of Information Science and Engineering Report, DMS-E95/81, 1995
7. Yue Z., Goshtasby A. and Ackerman V.L, "Automatic Detection of Rib Borders in Chest Radiographs", IEEE Transaction on Medical Imaging, 14(3):525-536
8. Sugahara T, Yanagihara Y. and Sugimoto N., "Construction of Structural Edge Map on Chest Radiograph using Hough Transformation and Line Connection", Systems and Computers in Japan, **26(6)**:71-78, 1995
9. Vogelsang F., Weiler F., Lesch T., Wein B. and Gunther R.W., "Compensation of Rib Structures in Digital X-rays of the Chest For Diagnose Assistance", Computer Assisted Radiology, 1020, 1996
10. Ginneken B. and Romeny B, "Automatic Delineation of Ribs in Frontal Chest Radiographs", Image Processing in SPIE, **3979**:825-826, 2000
11. Li Q., Katsuragawa S. and Doi K., "Improved Contralateral Subtraction Images by use of Elastic Matching Technique", Medical Physics, **27(8)**:1934-1942, 2000
12. Daponte S.J. and Fox D.M., "Enhancement of Chest Radiographs with Gradient Operators", IEEE Transactions on Medical Imaging, **7**:109-116, 1988
13. Brown Matthew., Wilson L., Doust B., Gill R., and Sun C., "Knowledge-Based Method for Segmentation and Analysis of Lung Boundaries in Chest X-ray images", Computerized medical imaging and graphics, **22**:463-477, 1998
14. Park M., Wilson L., and Jin J., "Automatic Extraction of Lung Boundaries by a Knowledge-Based Method", Visual Information Processing, **2**:14-19, 2001
15. Ishida T., Katsuragawa S., Nakamura K., MacMahon H. and Doi Kunio, "Iterative Image Warping Technique for Temporal Subtraction of Sequential Chest Radiographs to Detect Interval Change", Medical Physics" **26(7)**:1320-1329, 1999
16. Canny J. "A Computational Approach to Edge Detection", IEEE Transactions on Pattern Analysis and Machine Intelligence, 8(6):679-698, 1986
17. Gonzalez R.C. and Woods R.E., *Digital Image Processing*, Addison-Wesley Publishing Company, 1993